



HAL
open science

Initial Upper Palaeolithic Homo sapiens from Bacho Kiro Cave, Bulgaria

Jean-Jacques Hublin, Nikolay Sirakov, Vera Aldeias, Shara Bailey, Edouard Bard, Vincent Delvigne, Elena Endarova, Yoann Fagault, Helen Fewlass, Mateja Hajdinjak, et al.

► **To cite this version:**

Jean-Jacques Hublin, Nikolay Sirakov, Vera Aldeias, Shara Bailey, Edouard Bard, et al.. Initial Upper Palaeolithic Homo sapiens from Bacho Kiro Cave, Bulgaria. *Nature*, 2020, 581 (7808), pp.299-302. 10.1038/s41586-020-2259-z . hal-03321929

HAL Id: hal-03321929

<https://hal.inrae.fr/hal-03321929v1>

Submitted on 17 Sep 2021

HAL is a multi-disciplinary open access archive for the deposit and dissemination of scientific research documents, whether they are published or not. The documents may come from teaching and research institutions in France or abroad, or from public or private research centers.

L'archive ouverte pluridisciplinaire **HAL**, est destinée au dépôt et à la diffusion de documents scientifiques de niveau recherche, publiés ou non, émanant des établissements d'enseignement et de recherche français ou étrangers, des laboratoires publics ou privés.

Initial Upper Palaeolithic *Homo sapiens* from Bacho Kiro Cave, Bulgaria

Jean-Jacques Hublin^{1,2†}, Nikolay Sirakov³, Vera Aldeias⁴, Shara Bailey^{1,5}, Edouard Bard⁶, Vincent Delvigne^{7,8}, Elena Enderova⁹, Yoann Fagault⁶, Helen Fewlass¹, Mateja Hajdinjak¹⁰, Bernd Kromer¹, Ivaylo Krumov¹¹, João Marreiros^{4,12}, Naomi L. Martisius¹³, Lindsey Paskulin¹⁴, Virginie Sinet-Mathiot¹, Matthias Meyer¹⁰, Svante Pääbo¹⁰, Vasil Popov¹⁵, Zeljko Rezek^{1,16}, Svoboda Sirakova³, Matthew M. Skinner^{1,17}, Geoff M. Smith¹, Rosen Spasov¹⁸, Sahra Talamo^{1,19}, Thibaut Tuna⁶, Lukas Wacker²⁰, Frido Welker^{1,21}, Arndt Wilcke²², Nikolay Zahariev²³, Shannon P. McPherron¹ & Tsenka Tsanova¹

¹Department of Human Evolution, Max Planck Institute for Evolutionary Anthropology, Leipzig, Germany.

²Chaire Internationale de Paléoanthropologie, Collège de France, Paris, France.

³National Institute of Archaeology with Museum, Bulgarian Academy of Sciences, Sofia, Bulgaria.

⁴Interdisciplinary Centre for Archaeology and the Evolution of Human Behaviour, Universidade do Algarve, Faro, Portugal.

⁵Department of Anthropology, New York University, New York, NY, USA.

⁶CEREGE, CNRS, IRD, INRA, Collège de France, Université d'Aix Marseille, Aix-en-Provence, France.

⁷Service de Préhistoire, University of Liège, Liège, Belgium.

⁸CNRS, UMR 5199 PACEA, University of Bordeaux, Pessac, France.

⁹National History Museum, Sofia, Bulgaria.

¹⁰Department of Evolutionary Genetics, Max Planck Institute for Evolutionary Anthropology, Leipzig, Germany.

¹¹History Museum, Belogradchik, Bulgaria.

¹²TraCER, Monrepos Archaeological Research Centre and Museum for Human Behavioural Evolution, RGZM, Mainz, Germany.

¹³Department of Anthropology, University of California, Davis, Davis, CA, USA.

¹⁴Department of Archaeology, University of Aberdeen, Aberdeen, UK.

¹⁵Institute of Biodiversity and Ecosystem Research, Bulgarian Academy of Sciences, Sofia, Bulgaria.

¹⁶University of Pennsylvania Museum of Archaeology and Anthropology, Philadelphia, PA, USA.

¹⁷School of Anthropology and Conservation, University of Kent, Canterbury, UK.

¹⁸Archaeology Department, New Bulgarian University, Sofia, Bulgaria.

¹⁹Department of Chemistry 'G. Ciamician', University of Bologna, Bologna, Italy.

²⁰Department of Earth Sciences, ETH Zurich, Zurich, Switzerland.

²¹Section for Evolutionary Genomics, Globe Institute, University of Copenhagen, Copenhagen, Denmark.

²²Department of Cell Therapy, Fraunhofer Institute for Cell Therapy and Immunology, Leipzig, Germany.

The Middle-to-Upper Palaeolithic transition in Europe witnessed the replacement and partial absorption of local Neanderthal populations by *Homo sapiens* populations of African origin¹. However, this process probably varied across regions and the details of the scenario remain unknown. In particular, the duration of chronological overlap between the two groups is much debated, as are the implications of this overlap for the nature of the biological and cultural interactions between Neanderthals and *H. sapiens*. Here we report the discovery and direct dating of human remains found in association with Initial Upper Palaeolithic artefacts², from excavations at Bacho Kiro Cave (Bulgaria). Morphological analysis of a tooth and mitochondrial DNA from several hominin bone fragments, identified through proteomic screening, assign these finds to *H. sapiens* and link the expansion of Initial Upper Palaeolithic technologies with the spread of *H. sapiens* into the mid-latitudes of Eurasia before 45 thousand years ago³. The excavations yielded a wealth of bone artefacts, including pendants manufactured from cave bear teeth that are reminiscent of those later produced by the last Neanderthals of western Europe^{4–6}. These finds are consistent with models based on the arrival of multiple waves of *H. sapiens* into Europe, coming into contact with declining Neanderthal populations^{7,8}.

Fragmentary specimens from the sites of Kent's Cavern (United Kingdom)⁹ and Cavallo (Italy)¹⁰ have been claimed to document the earliest presence of our species in western Europe, between 44,200–41,500 calibrated years before present (cal. yr BP; taken as AD 1950) for the former and between 45,000–43,000 cal. yr BP for the latter. However, these dates are based on the archaeological contexts of the specimens rather than direct dating, and—in both cases—the exact stratigraphic origin of the fossils is debated^{11,12}. In the absence of directly dated fossil remains, reconstructing the timing of the expansions of *H. sapiens* into Europe rests on hypotheses concerning the makers of various so-called 'transitional' artefact assemblages at the advent of the Upper Palaeolithic period.

Bacho Kiro Cave is located 5 km west of Dryanovo (Bulgaria), on the northern slope of the Balkan mountain range (Stara Planina) and about 70 km south of the Danube River (Extended Data Fig. 1b). The site formed at the mouth of a large karstic system and its deposits encompass late Middle Palaeolithic and early Upper Palaeolithic occupations. Bacho Kiro Cave was excavated by D. Garrod in 1938, but is best known from more-extensive excavations (in 1971 to 1975) by a team led by B. Ginter and J. Kozłowski¹³. The excavations in the 1970s yielded fragmentary human remains¹³ that were subsequently lost. In 2015, the National Archaeological

Institute with Museum in Sofia and the Department of Human Evolution at the Max Planck Institute for Evolutionary Anthropology resumed work at Bacho Kiro Cave with the goals of clarifying the chronology (which had previously been based on a handful of inconsistent radiocarbon ages¹⁴) and the biological nature of the makers of the lithic assemblages. Two sectors with similar and well-preserved sequences were re-excavated: the ‘Main’ sector and the previously unexcavated ‘Niche 1’ sector, located on the south and east sides, respectively, of the excavation from the 1970s (Extended Data Fig. 1a). At the base of the sequence (Supplementary Information section 1) and overlying the bedrock, layer K has a relatively low density of Middle Palaeolithic artefacts. Sedimentologically, the contact of layer K with the overlying layer J is gradual and the artefact densities remain low; however, the upper part of layer J contains artefacts identical to those in layer I. On the basis of the radiocarbon dates³, layer J represents more than 3,000 years of accumulation. Layer I represents an intensification of the trends toward increased amounts of organic material and increased artefact seen in layer J. Layer I is an easily recognized and archaeologically rich organic deposit that spans from 45,820 to 43,650 cal. yr BP³ (95% modelled range) and yields an assemblage that was initially described as ‘Bachokirian’, but is now considered a variant of the Initial Upper Palaeolithic (IUP) industry¹⁵ (Extended Data Figs. 2–4, Supplementary Information section 2). Layer I is capped by water-laid deposits (layers H and G) that have little archaeological content. The overlying two metres of deposits in the Main sector contain low densities of Upper Palaeolithic artefacts.

We found a hominin second lower molar (specimen code F6-620) (Extended Data Fig. 5a) in the upper part of layer J. The crown dimensions of this tooth place it at the high end of both the Neanderthal and the Upper Palaeolithic *H. sapiens* range (Extended Data Table 1). With the exception of a moderately expressed—but divided—middle trigonid crest, all of the morphological trait expressions found in F6-620 align the tooth with *H. sapiens* (Supplementary Information section 3). The expression of a middle trigonid crest observed on the Bacho Kiro second lower molar is present in 10% of these teeth in some groups of humans¹⁶ and in 8% of early *H. sapiens*¹⁷. The pulp chamber is hypotaurodont¹⁸, a condition that is common in some recent human groups¹⁹ and is unlike the hypertaurodont molars of Neanderthals²⁰. The four-cusp configuration of the Bacho Kiro second lower molar is absent in Neanderthals. Our geometric morphometric analysis of the enamel–dentine junction also clearly assigns the specimen to *H. sapiens* (Extended Data Fig. 5b).

We screened 1,271 non-identifiable bones and teeth using matrix-assisted laser desorption–ionization time-of-flight mass spectrometry (MALDI–TOF–MS) collagen-peptide mass fingerprinting (also known as ZooMS²¹) to identify hominin remains, with the aim of

providing accurate molecular identifications for radiocarbon-dated specimens and of enlarging our understanding of the species composition of the fauna. ZooMS screening identified six hominin bone fragments (Extended Data Fig. 6, Supplementary Information section 4), of which four come from layer I in Niche 1, one from layer B in the Main sector (Extended Data Fig. 1) and one from the layer 6a/7 of the excavations in the 1970s¹³. Including the F6-620 tooth, we recovered five hominin specimens in total from the IUP layers. The calibrated radiocarbon dates of the 4 ZooMS-identified human fragments range from 46,790 to 42,810 cal. yr BP at 95.4% probability (Fig. 1). These ages are in full agreement with the modelled boundaries of layer I (45,820–43,650 cal. yr BP at 95.4%), which includes the 4 humans and 21 other dates on modified fauna³. Therefore, to our knowledge, these bones represent the oldest European Upper Palaeolithic hominins recovered to date.

We extracted DNA^{22,23} from F6-620 and the six hominin bone fragments identified using ZooMS. We performed library preparation²⁴, enrichment of human mitochondrial DNA (mtDNA)²⁵ and sequencing, which enabled us to recover between 13,856 and 795,043 unique mtDNA fragments (Supplementary Information section 5). The frequencies of cytosine-to-thymine substitutions, which are characteristic of ancient-DNA base damage, ranged from 13.5% to 54.9% at the 5' ends and from 9.4% to 42.2% at the 3' ends of these fragments (Extended Data Fig. 7), which suggests that at least some of the fragments are of ancient origin. After restricting analyses to putatively deaminated DNA fragments to remove contamination by recent human DNA, sequence coverage of the mitochondrial genome enabled us to reconstruct six full mitochondrial genomes out of seven. The mtDNA sequences of F6-620 and one of the ZooMS-identified hominin bone fragments (AA7-738) are identical, which indicates that these specimens belonged either to the same individual or to two maternally related individuals. In a tree relating these mtDNA genomes to the known mtDNA sequences of 54 present-day humans, 12 ancient *H. sapiens*, 22 Neanderthals, 4 Denisovans and a hominin from Sima de los Huesos, all of the Bacho Kiro Cave mtDNA genomes fall within the variation of *H. sapiens* (Fig. 2, Extended Data Fig. 8). The specimens from layer I yielded mtDNA sequences that fall close to the base of each of the three major macro-haplogroups of present-day non-Africans (M, N and R). Although the mtDNA sequences belong to different macro-haplogroups, they differ (at most) at 15 positions from each other—which is lower than the differences observed among 97.5% of contemporary European individuals who are not closely related to one another²⁶. The older Bacho Kiro population contains early representatives of the macro-haplogroup M, which is not present in Europe today²⁷. Furthermore, the mtDNA genomes of the Bacho Kiro Cave specimens accumulated fewer substitutions than those of present-day humans. Using 10 directly dated

ancient *H. sapiens* as calibration points^{28,29} (Supplementary Information section 5), we obtained genetic dates that range from 44,830 to 42,616 yr BP for the layer-I hominins (Extended Data Table 2), in good agreement with the calibrated radiocarbon dates (Fig. 1).

The fauna associated with these *H. sapiens* specimens (layers I and J, $n = 11,259$) includes 23 species, dominated by *Bos* or *Bison*, cervids and caprines, alongside equids (Supplementary Information section 6). The species composition comprises a mix of taxa adapted to cold or to warmer environments, characteristic of the faunal record in marine isotope stage 3 in the Balkans^{30,31}. A variety of carnivores are also present, dominated by cave bear (*Ursus spelaeus*). Zooarchaeological analyses strongly indicate that the accumulation of the fauna is predominantly anthropogenic. One notable aspect of the faunal assemblage is the presence of numerous anthropogenically modified objects (Fig. 3, Supplementary Information section 6): worked pieces include awls, *lissoirs* ('smoothers') and incised pieces. Several of the artefacts have red staining that is consistent with the use of ochre. We identified 1 perforated ivory bead and 12 perforated or grooved pendants, 11 of which were made from cave bear teeth and 1 from an ungulate tooth (Fig. 3).

The stone tools associated with *H. sapiens* in layer I were initially assigned to the Bachokirian industry because they did not fit comfortably with either the Middle Palaeolithic or Aurignacian-like Upper Palaeolithic techno-complexes: however, we now know that these stone tools fit within the IUP assemblages¹⁵. IUP assemblages—similar to that of Bacho Kiro Cave (Supplementary Information section 2)—are characterized by blades and tool types typical of Upper Palaeolithic industries, but with some Levallois forms and faceted platforms that are reminiscent of lithics of the preceding Middle Palaeolithic and African Middle Stone Age² (Extended Data Figs. 3, 4). IUP assemblages, which span Eurasia from central Europe to Mongolia, occur before the appearance of Upper Palaeolithic assemblages characterized by bladelet production, and arguably have their origin in southwest Asia (Extended Data Fig. 2). The Bacho Kiro Cave IUP is similar to the IUP from layers I and F at Üçağızlı Cave (Turkey) in terms of lithic technology, typology, and the presence of shaped bone tools and pendants, as well as with respect to ages^{32,33}.

The Bacho Kiro Cave site clearly demonstrates that the IUP techno-complex in this region was made by *H. sapiens*, and is consistent with models that attribute the spread of these technologies to the dispersal of our species throughout large parts of Eurasia at this time. The presence of IUP assemblages documents a wave of peopling that precedes the spread of the first Upper Palaeolithic bladelet techno-complexes—such as the Early Ahmarian industry in the

Levant, the Early Kozarnikan industry in the eastern Balkans and the Protoaurignacian industry in western and central Europe—by several millennia^{1,34}. At Bacho Kiro Cave, the IUP assemblage starts before 45,000 cal. yr BP and, as the assemblage of the upper part of layer J is identical to that from layer I, it may begin as early as 47,000 cal. yr BP³. We now have evidence for *H. sapiens* in Eurasia spanning from Ust'-Ishim²⁸ in western Siberia to Bacho Kiro Cave in eastern Europe, directly dated to approximately 45,000 cal. yr BP. Together, the behavioural and biological evidence strongly suggest a relatively rapid dispersal of IUP assemblages from southwest Asia³⁵ into mid-latitude Eurasia by groups that—contrary to Aurignacian populations—seem unrelated to present-day European populations²⁸. Direct contact with Neanderthals must have occurred much earlier in eastern Europe than in western Europe, where the latest Neanderthals and their associated assemblages persisted until at least about 40,000 cal. yr BP^{1,5,6}. In Romania, the Peștera cu Oase *H. sapiens* individual had a Neanderthal ancestor as recently as four-to-six generations back in his family tree³⁶. In light of the Bacho Kiro Cave results, the 42,000–37,000 cal. yr BP radiocarbon age of the Peștera cu Oase fossil implies an extended period of contact between Neanderthals and *H. sapiens* in eastern Europe. Alternatively, it may be that the direct date of Peștera cu Oase—which was obtained before recent improvements in pretreatment techniques—is an underestimate, and that local coexistence was more ancient and ephemeral. The IUP pendants of Bacho Kiro Cave (Fig. 3) are notably similar to artefacts produced by late Neanderthals of the Châtelperronian layers at Grotte du Renne (France)⁴. Whatever the cognitive complexity of the last Neanderthals might have been, the earlier age of the Bacho Kiro Cave material supports the notion that the specific behavioural novelties seen in these Neanderthal populations resulted from contacts with migrant *H. sapiens*⁷.

Online content Any methods, additional references, Nature Research reporting summaries, source data, extended data, supplementary information, acknowledgements, peer review information; details of author contributions and competing interests; and statements of data and code availability are available at

Received 30 July 2019; accepted 24 February 2020

- <jrn>1. Hublin, J.-J. The modern human colonization of western Eurasia: when and where? *Quat. Sci. Rev.* **118**, 194–210 (2015). </jrn>
- <jrn>2. Kuhn, S. L. & Zwyns, N. Rethinking the initial Upper Paleolithic. *Quat. Int.* **347**, 29–38 (2014). </jrn>
- <jrn>3. Fewlass, H. et al. New ¹⁴C chronology for Middle-to-Upper Palaeolithic transition at Bacho Kiro cave, Bulgaria. *Nat. Ecol. Evol.* (submitted for review)

- <jrn>4. White, R. Personal ornaments from the Grotte du Renne at Arcy-sur-Cure. *Athena Review* **2**, 41–46 (2001). </jrn>
- <jrn>5. Welker, F. et al. Palaeoproteomic evidence identifies archaic hominins associated with the Châtelperronian at the Grotte du Renne. *Proc. Natl Acad. Sci. USA* **113**, 11162–11167 (2016). </jrn>
- <jrn>6. Hublin, J.-J. et al. Radiocarbon dates from the Grotte du Renne and Saint-Césaire support a Neanderthal origin for the Châtelperronian. *Proc. Natl Acad. Sci. USA* **109**, 18743–18748 (2012). </jrn>
- <jrn>7. Hublin, J.-J., Spoor, F., Braun, M., Zonneveld, F. & Condemi, S. A late Neanderthal associated with Upper Palaeolithic artefacts. *Nature* **381**, 224–226 (1996). </jrn>
- <jrn>8. Ruebens, K., McPherron, S. J. P. & Hublin, J.-J. On the local Mousterian origin of the Châtelperronian: integrating typo-technological, chronostratigraphic and contextual data. *J. Hum. Evol.* **86**, 55–91 (2015). </jrn>
- <jrn>9. Higham, T. et al. The earliest evidence for anatomically modern humans in northwestern Europe. *Nature* **479**, 521–524 (2011). </jrn>
- <jrn>10. Benazzi, S. et al. Early dispersal of modern humans in Europe and implications for Neanderthal behaviour. *Nature* **479**, 525–528 (2011). </jrn>
- <jrn>11. White, M. & Pettitt, P. Ancient digs and modern myths: the age and context of the Kent's Cavern 4 maxilla and the earliest *Homo sapiens* specimens in Europe. *Eur. J. Archaeol.* **15**, 392–420 (2012). </jrn>
- <jrn>12. Zilhão, J., Banks, W. E., d'Errico, F. & Gioia, P. Analysis of site formation and assemblage integrity does not support attribution of the Uluzzian to modern humans at Grotta del Cavallo. *PLoS ONE* **10**, e0131181 (2015). </jrn>
- <other>13. Kozłowski, J. K. *Excavation in the Bacho Kiro Cave (Bulgaria): Final Report*. 172 (Panstwowe Wydawnictwo Naukowe, 1982). </other>
- <jrn>14. Hedges, R. E. M., Housley, R. A., Bronk, R. C. & Klinken, G. J. V. Radiocarbon dates from the Oxford AMS system: archaeometry datelist 18. *Archaeometry* **36**, 337–374 (1994). </jrn>
- <conf>15. Tsanova, T. & Bordes, J. G. in *The Humanized Mineral World: Towards Social and Symbolic Evaluation of Prehistoric Technologies in South Eastern Europe*

(*Proceedings of the ESF Workshop*) (eds Tsonev, T. S. & Montagnari Kokclj, E.) 41–50 (ERAUL, 2003).</conf>

- <jrn>16. Bailey, S. E. A closer look at Neanderthal postcanine dental morphology: the mandibular dentition. *Anat. Rec.* **269**, 148–156 (2002). </jrn>
- <jrn>17. Bailey, S. E., Skinner, M. M. & Hublin, J.-J. What lies beneath? An evaluation of lower molar trigonid crest patterns based on both dentine and enamel expression. *Am. J. Phys. Anthropol.* **145**, 505–518 (2011). </jrn>
- <jrn>18. Keith, A. Problems relating to the teeth of the earlier forms of prehistoric man. *Proc. R. Soc. Med.* **6**, 103–124 (1913). </jrn>
- <bok>19. Shaw, J. *The Teeth, the Bony Palate and the Mandible in Bantu Races of South Africa* (Bale and Danielsson, London, 1938).</bok>
- <edb>20. Kallay, J. in *Dental Anthropology* (ed. Brothwell, D.) 75–86, 1963.</edb>
- <jrn>21. Buckley, M., Collins, M., Thomas-Oates, J. & Wilson, J. C. Species identification by analysis of bone collagen using matrix-assisted laser desorption/ionisation time-of-flight mass spectrometry. *Rapid Commun. Mass Spectrom.* **23**, 3843–3854 (2009). </jrn>
- <jrn>22. Dabney, J. et al. Complete mitochondrial genome sequence of a Middle Pleistocene cave bear reconstructed from ultrashort DNA fragments. *Proc. Natl Acad. Sci. USA* **110**, 15758–15763 (2013). </jrn>
- <jrn>23. Korlević, P. et al. Reducing microbial and human contamination in DNA extractions from ancient bones and teeth. *Biotechniques* **59**, 87–93 (2015). </jrn>
- <jrn>24. Gansauge, M.-T. et al. Single-stranded DNA library preparation from highly degraded DNA using T4 DNA ligase. *Nucleic Acids Res.* **45**, e79 (2017). </jrn>
- <jrn>25. Fu, Q. et al. DNA analysis of an early modern human from Tianyuan Cave, China. *Proc. Natl Acad. Sci. USA* **110**, 2223–2227 (2013). </jrn>
- <jrn>26. Lippold, S. et al. Human paternal and maternal demographic histories: insights from high-resolution Y chromosome and mtDNA sequences. *Investig. Genet.* **5**, 13 (2014). </jrn>
- <jrn>27. Kivisild, T. Maternal ancestry and population history from whole mitochondrial genomes. *Investig. Genet.* **6**, 3 (2015). </jrn>
- <jrn>28. Fu, Q. et al. Genome sequence of a 45,000-year-old modern human from western Siberia. *Nature* **514**, 445–449 (2014). </jrn>

- <jrn>29. Fu, Q. et al. A revised timescale for human evolution based on ancient mitochondrial genomes. *Curr. Biol.* **23**, 553–559 (2013). </jrn>
- <edb>30. van der Made, J. in *The Encyclopedia of Archaeological Sciences* (ed. López Varela, S. L.) 1–4 (Wiley-Blackwell, 2018).</edb>
- <jrn>31. Guérin, C. Première biozonation du Pléistocène Européen, principal résultat biostratigraphique de l'étude des Rhinocerotidae (Mammalia, Perissodactyla) du Miocène terminal au Pléistocène supérieur d'Europe Occidentale. *Geobios* **15**, 593–598 (1982). </jrn>
- <jrn>32. Kuhn, S. L. et al. The early Upper Paleolithic occupations at Uçağizli Cave (Hatay, Turkey). *J. Hum. Evol.* **56**, 87–113 (2009). </jrn>
- <jrn>33. Kuhn, S. L. Upper Paleolithic raw material economies at Üçağizh cave, Turkey. *J. Anthropol. Archaeol.* **23**, 431–448 (2004). </jrn>
- <jrn>34. Müller, U. C. et al. The role of climate in the spread of modern humans into Europe. *Quat. Sci. Rev.* **30**, 273–279 (2011). </jrn>
- <jrn>35. Hershkovitz, I. et al. Levantine cranium from Manot Cave (Israel) foreshadows the first European modern humans. *Nature* **520**, 216–219 (2015). </jrn>
- <jrn>36. Fu, Q. et al. An early modern human from Romania with a recent Neanderthal ancestor. *Nature* **524**, 216–219 (2015). </jrn>

Châtelperronian Late Neanderthals

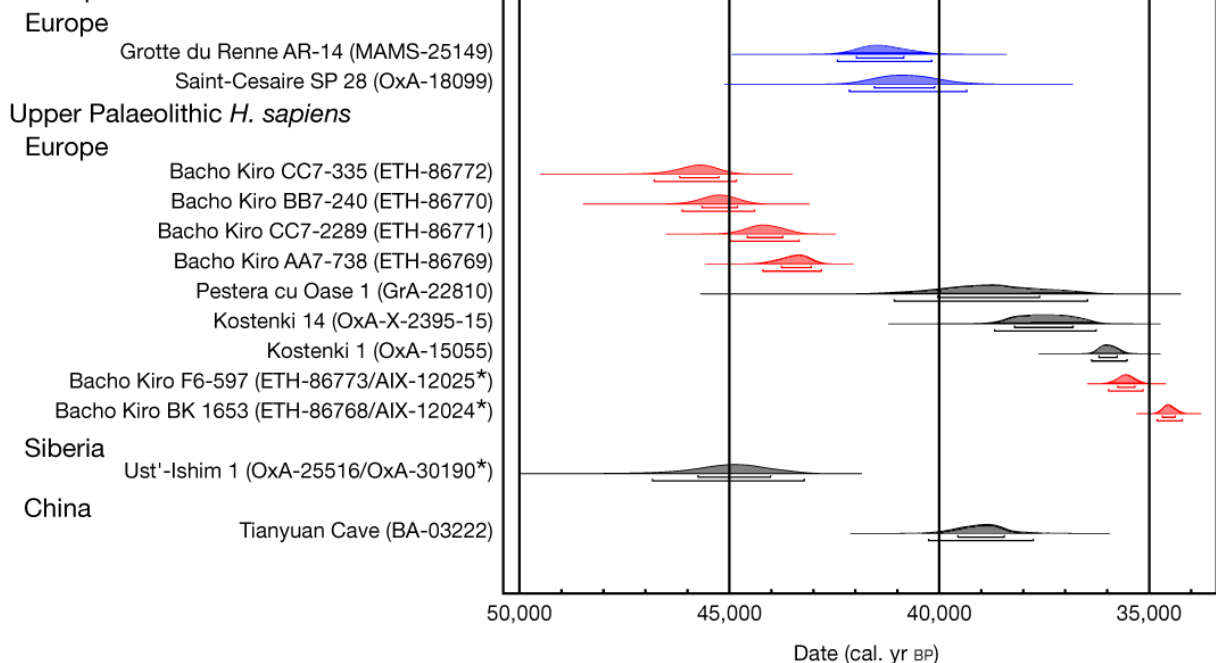


Fig. 1 | Direct dates for hominins of the Middle-to-Upper Palaeolithic transition in Europe. Directly dated Châtelperronian Neanderthals (blue) and *H. sapiens* (red or black) of the Middle-to-Upper Palaeolithic transition in Eurasia. The dates from Bacho Kiro Cave (red) have previously been reported³, as part of an extensive site chronology. Asterisks mark the dates that were combined using the R_Combine function in OxCal v.4.3. Codes in parentheses refer to dating sample identifiers; all the dates shown here are in Supplementary Table 16, with sample information and references.

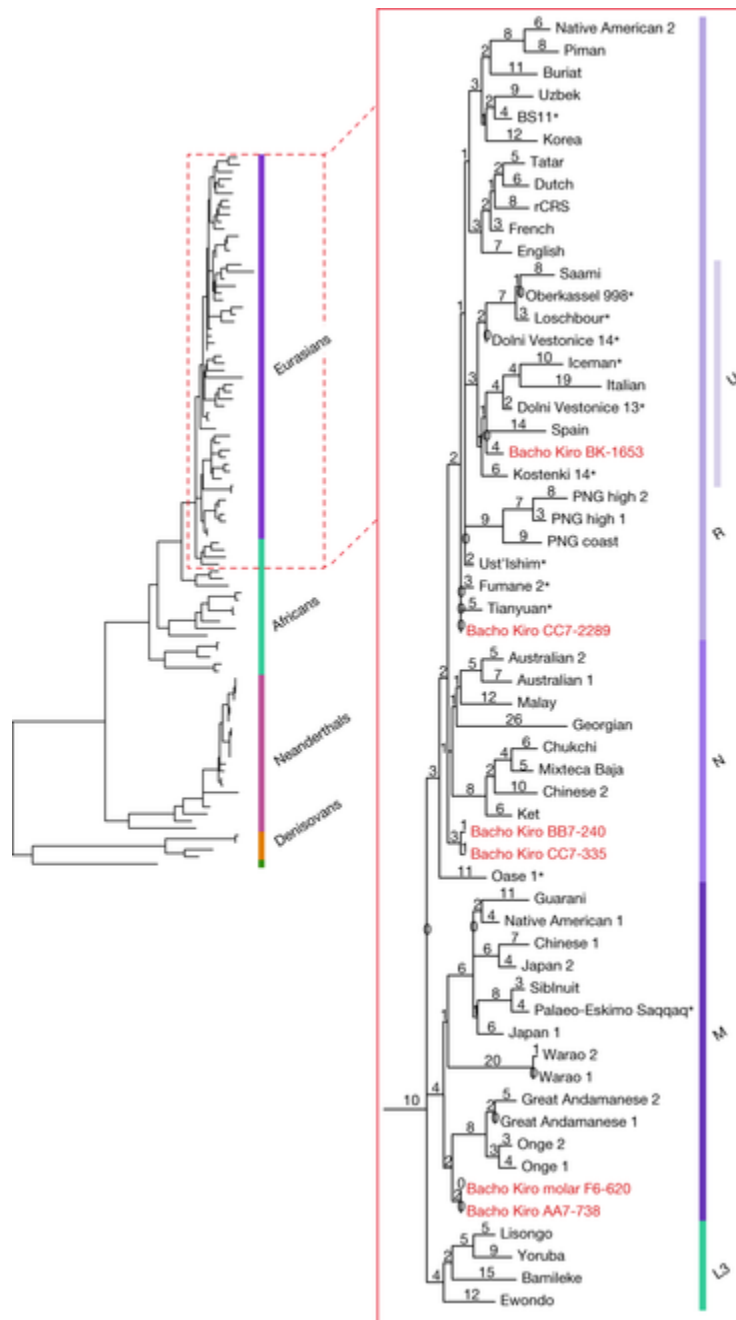


Fig. 2 | Maximum parsimony tree. Maximum parsimony tree relating Bacho Kiro Cave mtDNAs to 54 present-day humans, 12 ancient *H. sapiens*, 22 Neanderthals, 4 Denisovans and 1 individual from Sima de los Huesos. The insert shows the part of the tree closest to the

mtDNAs of the specimens from Bacho Kiro Cave. Bacho Kiro Cave mtDNAs are red. Asterisks denote mtDNA from ancient *H. sapiens* (Supplementary Table 9) other than the Bacho Kiro Cave specimens. The number of inferred substitutions per sequence is given above each branch. A chimpanzee mtDNA sequence was used to root the tree (not shown). rCRS, revised Cambridge Reference Sequence. U, R, N, M and L3 refer to the mitochondrial haplogroups.



Fig. 3 | Animal bone tools and personal ornaments from Bacho Kiro Cave layers I and J (Niche 1 and Main sectors). a–j, Pendants made from perforated and grooved teeth (a, ungulate; b–j, cave bear). k, l, o, Awls. m, Anthropogenically modified piece. n, p, Lissoirs. q, ivory bead. Further details are provided in Supplementary Table 15. Scale bars, 1 cm (a–o, q), 3 cm (p)

METHODS

No statistical methods were used to predetermine sample size. The experiments were not randomized and investigators were not blinded to allocation during experiments and outcome assessment.

Excavation methods

The site was excavated closely following existing protocols^{37–42}. Layers were defined first on lithological criteria, and second on archaeological criteria. Our stratigraphy was determined and named independently of previous excavations¹³. Additionally, we excavated in two unconnected areas of the site, and thus separate naming conventions were used between these two areas. The excavations in the south area (Extended Data Fig. 1) are known as the Main sector, and the layers are named with letters for the large divisions and numbers for divisions within these (for example, layer I or layer A0). The other area excavated is a niche to the east of the previous excavations. We call this area Niche 1 (or N1), and all layer names from this area are prefixed with N1-. Where we hypothesize a link between the two sectors, we use the same layer name (for example, layers N1-I and I). Where we are unable to form a strong hypothesis about the link between the two sectors, we use different layer names (numbers in this case) in the Niche 1 sector to denote this (for example, N1-3), followed by letter for internal subdivisions (for example, N1-3a). All finds were recorded by layer and 3D coordinates (using an arbitrary grid established for the excavation and aligned to the previous excavations) measured with Leica total stations (5'' accuracy) using data collectors with self-authored software (EDM-Mobile). All lithics and fauna >20 mm in length and all specialists' samples (for example, ancient DNA, micromorphology, phytoliths and so on) were provenienced and given unique identifiers (IDs). Complete bones, identifiable teeth and human remains <20 mm in length (but larger than microfauna) were also given coordinates and IDs. Natural stones >10 cm in length were recorded with a single coordinate, and stones >20 cm in length were measured with multiple coordinates to describe their volume and orientation. The sediment, excluding recorded stones and artefacts, was collected by 9-l buckets and wet-screened on-site through 6- and 1.2-mm meshes to form two fractions. Buckets have unique IDs. Their coordinates were measured first in the centre of the area to be excavated and then again at the centre of the area excavated at the completion of the bucket. Large (>20-mm-long) objects found in the sediment in the buckets during wet-screening were given IDs and assigned the coordinates of the bucket. All features were provenienced. Digital photographs documenting the excavation were recorded daily, and final sections were documented through a combination of digital photography, drawing, and total station measures.

Additionally, structure-from-motion models were made of all final sections and excavation areas. These models were georeferenced to the excavation grid using total station coordinates.

ZooMS

We screened 1,271 fragmentary bone and tooth specimens from Bacho Kiro Cave using ZooMS²¹. Eleven bone specimens were derived from the previous excavations at the site¹³, 371 from our excavations in the Main sector, and 889 bone specimens from the Niche 1 area. We particularly focused on IUP layers I and N1-I ($n = 822$). Extraction and analytical protocols followed previously published work⁵. In short, a small bone sample (<20 mg) was taken from each bone or dentine specimen. The sample was incubated at 65 °C for an hour in 50 mM ammonium-bicarbonate buffer, digested overnight using trypsin (Promega) at 37 °C, acidified using 0.2 20% TFA, and cleaned on C18 ZipTips (either from Sigma-Aldrich or Thermo Scientific). MALDI–TOF–MS analysis was conducted at the IZI Fraunhofer in Leipzig⁴³. MALDI–TOF–MS spectra were analysed in comparison to a reference database containing collagen-peptide marker masses of all medium- to larger-sized genera in existence in western Eurasia during the Late Pleistocene epoch⁵. In cases in which ammonium-bicarbonate extraction failed, an attempt was made to recover further informative collagen peptides through acid demineralization of the same bone sample, as previously explained⁵. Collagen deamidation in these spectra was assessed for two peptides (P1105 and P1706)^{44,45}.

Bone pretreatment and accelerated mass spectrometry dating

Small aliquots (80–110 mg) of the six ZooMS-identified hominin bone fragments were sampled to preserve as much material as possible for further analyses. Collagen was extracted using a previously described technique⁴⁶ for small bone sample sizes, based on a modified previously published collagen-extraction protocol⁴⁷ followed by an ultrafiltration step⁴⁸. In brief, the outer surfaces of the bone samples were removed with a sandblaster, and samples were removed using a rotary tool. The bones were demineralized in 0.5 M HCl at 4 °C until soft and CO₂ effervescence had stopped. Then, 0.1 M NaOH was added for 10 min at room temperature to remove humic acid contamination, and samples were re-acidified in 0.5M HCl. The collagen was gelatinized in acidic water (HCl pH 3) at 70 °C for several hours (4–6 h). The collagen samples were then passed through an Ezee Filter (Elkay Laboratories) to remove large particles (>80 µm) and separated by molecular weight with pre-cleaned Sartorius VivaSpin Turbo 15 ultrafilters (30-kDa molecular weight cut-off (MWCO))^{49,50}. The samples were freeze-dried and the large molecular fraction (>30 kDa) was graphitized using Automated Graphitisation Equipment III⁵¹ and measured using the latest model of the MICADAS accelerated mass spectrometry (AMS)⁵² in the Laboratory of Ion Beam Physics at ETH-Zurich (laboratory code ETH). Small aliquots

(66–89 mg) of a background cave bear bone (>50,000 yr BP) were extracted alongside the samples to monitor contamination introduced in the laboratory⁵³. These were measured in the same magazine as the hominin samples and used in the age calculation. Oxalic acid II standards were also measured in the same magazine and used for normalization. Data reduction was performed using BATS software⁵⁴. An additional 1‰ was added to the error calculation of the samples, as per standard practice. The dates were calibrated using the IntCal13⁵⁵ dataset in OxCal v.4.3⁵⁶.

Shape analysis of the molar enamel–dentine junction

Enamel and dentine tissues (Extended Data Fig. 5) of lower second molars were segmented using the 3D voxel value histogram and its distribution of greyscale values^{50,51}. After segmentation, the enamel–dentine junction was reconstructed as a triangle-based surface model using Avizo. Small enamel–dentine junction defects were corrected digitally using the ‘fill holes’ module of Geomagic Studio. We then used Avizo to digitize 3D landmarks and curve-semilandmarks on the enamel–dentine junction surface^{50,51}. Anatomical landmarks were placed on the tip of the dentine horn of the protoconid, metaconid, entoconid and hypoconid. A sequence of landmarks was also placed along the marginal ridge connecting the dentine horns, beginning at the top of the protoconid and moving in lingual direction; the points along this ridge curve were then later resampled to the same point count on every specimen using Mathematica. Likewise, we digitized and resampled a curve along the cemento–enamel junction as a closed curve starting and ending below the protoconid horn and the mesiobuccal corner of the cervix. The resampled points along the two ridge curves were subsequently treated as sliding curve semilandmarks and analysed using geometric morphometrics together with the four anatomical landmarks. Landmarks not preserved on the Bacho Kiro Cave specimen were removed before principal component analysis. The specimens of *Homo erectus* sensu lato include KNM-ER 1802, KNM-ER 992 and Sangiran 1b. Specimens of archaic Middle Pleistocene hominins include Balanica 1, Mauer, Xiahe and KNM-ER BK 67. The Neanderthal sample includes Abri Suard S36, Krapina 1, 6, 9, 53, 54, 55, 57, 59, 80, 86, 105 and 107, La Quina H9, Le Moustier 1, Regourdou, Scladina 4A1, El Sidron 540 and 755, and Vindija 11-39. The fossil *H. sapiens* sample includes Dar es Soltane II H4, El Harhoura, Jebel Irhoud 3 and 11, Qafzeh 9, 10, 11 and 15, and Temara. The recent *H. sapiens* sample includes clinical extractions from dentists based in Germany, Neolithic specimens from Belgium (Royal Belgian Institute of Natural Sciences) and specimens from the Francisc J. Rainer Collection (Institutul de Antropologie ‘Francisc J. Rainer’).

DNA extraction and library preparation

Samples of between 29.3 mg and 64.7 mg of tooth or bone powder were removed from 7 Bacho Kiro Cave specimens (F6-620, AA7-738, BB7-240, CC7-2289, CC7-335, F6-597 and BK-1653) using a sterile dentistry drill (Supplementary Table 4) after a thin layer of surface was removed from the sampling areas. DNA was extracted from the powder using a silica-based method²² as previously described²³. Five single-stranded DNA libraries²⁴ were made from 10 µl from each extract on an automated liquid handling platform (Bravo NGS workstation B, Agilent Technologies)⁵⁹. A control oligonucleotide was spiked into each reaction to determine the efficiency of library preparation⁶⁰, and quantitative PCR was used to determine the total number of unique library molecules as well as the number of oligonucleotides that were successfully converted^{24,60}. The libraries were amplified into plateau with AccuPrime Pfx DNA polymerase (Life Technologies)⁶¹ and labelled with two unique indices^{23,62}. Half of the volume of the amplified libraries (50 µl) was purified using SPRI beads on the automated liquid handling platform⁵⁹. The concentrations of the purified DNA libraries were determined using a NanoDrop Spectrophotometer (NanoDrop Technologies).

mtDNA capture and sequencing

An aliquot of each amplified library was enriched for human mtDNA using a bead-based hybridization method²⁹. Enriched libraries were sequenced on an Illumina MiSeq platform in a double index configuration (2 × 76 cycles)⁶² and base-calling was done using Bustard (Illumina). Overlapping paired-end reads were merged into single sequences and the adapters were trimmed using leeHom⁶³. The Burrows–Wheeler Aligner (BWA, version: 0.5.10-evan.9-1-g44db244; <https://github.com/mpieva/network-aware-bwa>)⁶⁴, with parameters adjusted for ancient DNA (‘-n 0.01 -o 2 -l 16500’)⁶⁵, was used to align the data to the revised Cambridge Reference Sequence (NC_01290). Only reads with perfect matches to the expected index combinations were retained for downstream analyses. PCR duplicates were removed using bam-rmdup (version 0.6.3; <https://bitbucket.org/ustenzel/biohazard>). SAMtools (version 1.3.1)⁶⁶ was used to filter for fragments that were longer than 35 base pairs and that had a mapping quality of at least 25. We merged the libraries originating from the same extract (that is, the same specimen) using SAMtools merge to produce the final dataset.

Phylogenetic inferences

We reconstructed the mitochondrial genomes of the Bacho Kiro Cave specimens once by using all mapped fragments longer than 35 base pairs with a mapping quality of at least 25 and once using only fragments with a cytosine (C) to thymine (T) difference to the reference genome at the first three and/or last three terminal positions³⁶ (that is, putatively deaminated fragments). We

called a consensus base at each position along the mtDNA that was covered by at least 3 DNA fragments and at which at least 2/3 of fragments carried an identical base and the base quality was 20 or higher⁶⁷. To prevent deamination-induced substitutions affecting the calling of a consensus base, we converted A on the reverse strands and T on the forward strands in the first three and the last three positions of a fragment into N.

The libraries prepared from the F6-597 specimen yielded too few informative mtDNA fragments to reconstruct a complete mtDNA using putatively deaminated fragments. We investigated the state of F6-597 DNA fragments that overlapped positions ‘diagnostic’ for each branch in a mtDNA tree relating present-day humans, Neanderthals, Denisovans and the hominin from Sima de los Huesos⁶⁸ (Supplementary Table 6). To diminish the influence of substitutions derived from deamination, all forward strands were ignored if one of the possible states at an informative state was a C and all reverse strands were ignored if one of the possible states was G.

We aligned the reconstructed mitochondrial genomes of the Bacho Kiro Cave individuals to the mtDNA genomes of 54 present-day humans from a wide geographical distribution⁶⁹, 12 ancient *H. sapiens*^{25,28,41,70–73} (Supplementary Table 9), 22 Neanderthals^{69,74–78}, 4 Denisovans^{79–82}, a Sima de los Huesos individual⁶⁷ and a chimpanzee⁸³ using MAFFT v.7.271⁸⁴. The number of pairwise differences among the genomes was calculated using MEGA7⁸⁵ and a maximum parsimony tree was reconstructed using Parsimony ratchet as implemented in the R package phangorn⁸⁶. We identified the haplogroup of each of the reconstructed mitochondrial genomes with HaploGrep⁸⁷ based on the PhyloTree database (PhyloTree.org, build 17).

Contamination estimates

We used two complementary approaches to estimate levels of present-day human mtDNA contamination in the libraries. We identified positions at which each of the reconstructed Bacho Kiro Cave mtDNAs differ from at least 99% of a world-wide panel of 311 present-day human mtDNAs^{36,69} (Supplementary Tables 7, 8). We then counted DNA fragments that overlap these positions and did not match the consensus base of the respective specimen, again taking into account the strand orientation in cases in which one of the possible states at an informative site was C or G. In the second approach, we used an iterative probabilistic method, schmutzi⁸⁸, which uses a nonredundant database of human mitochondrial genomes to estimate levels of present-day human DNA contamination (Supplementary Information section 5) (parameters: ‘—notusepredC —uselength’).

Molecular DNA dating

We estimated the tip dates of the reconstructed Bacho Kiro Cave mtDNAs using the Bayesian phylogenetic method as implemented in BEAST2 (version 2.4.8)⁸⁹ by aligning the reconstructed mitochondrial genomes to 54 present-day humans and 10 directly radiocarbon-dated ancient *H. sapiens*^{28,29,72,73,80}, which were used for tip calibration. The Neanderthal mtDNA genome of Vindija 33.16⁶⁹ was used as an outgroup. The best-fitting substitution model was determined using jModelTest2⁹⁰. We investigated a strict clock and an uncorrelated log-normal relaxed clock as two models of rate variation and a constant population size and a Bayesian skyline as tree priors²⁸. For each model, we carried out Markov chain Monte Carlo runs with 30,000,000 iterations and sampling every 1,000 steps. After discarding 10% of the iterations as burn-in, the output was analysed with Tracer v.1.5.0 (<http://tree.bio.ed.ac.uk/software/tracer/>). A marginal likelihood estimation⁹¹ analysis was used for model comparison and best support assessment. Both the maximum parsimony and the BEAST2 tree were visualized with FigTree (version v.1.4.2) (<http://tree.bio.ed.ac.uk/software/figtree/>).

Micromorphology

Field observations of the sediments were complemented by archaeological micromorphology analyses. Micromorphological samples were collected as undisturbed blocks by carefully carving and wrapping them with either pre-plastered bandages or soft paper and tape. Thin sections were manufactured by Spectrum Petrographics through a standard procedure of drying the blocks in an oven for several days at about 60 °C. The blocks were then impregnated with a mixture of polyester resin and styrene, to which a catalyst was added. Thin sections were ground to a thickness of 30 µm and observed under a petrographic microscope in plane- and cross-polarized light at magnifications ranging from 20× to 400×. Micromorphological nomenclature follows previously published work^{92,93}.

Reporting summary

Further information on research design is available in the Nature Research Reporting Summary linked to this paper.

Data availability

The data that support the findings of this study are available from the corresponding authors upon reasonable request. Genetic sequence reads from all libraries and corresponding negative controls are deposited at European Nucleotide Archive under the study accession number [PRJEB35466](https://www.ebi.ac.uk/ena/record/PRJEB35466). The FASTA files of the mitochondrial genomes are deposited in GenBank with the accession numbers MN706602–MN706607. Details are as follows: Bacho Kiro AA7-738, [MN706602](https://www.ncbi.nlm.nih.gov/nuccore/MN706602);

Bacho Kiro BB7-240, [MN706603](#); Bacho Kiro BK-1653, [MN706604](#); Bacho Kiro CC7-335, [MN706605](#); Bacho Kiro CC7-2289, [MN706606](#); and Bacho Kiro molar F6-620, [MN706607](#).

<bok>37. Dibble, H. L. & Lenoir, M. *The Middle Paleolithic Site of Combe-Capelle Bas (France)* (The University Museum Press, 1995).</bok>

<edb>38. Turq, A. et al. in *Les Sociétés du Paléolithique dans un Grand Sud-ouest de la France: Nouveaux Gisements, Nouveaux Résultats, Nouvelles Méthodes* (eds. Jaubert, J. et al.) 83–94 (Mémoire de la Société Préhistorique Française, 2008).</edb>

<edb>39. Chase, P. G., Debénath, A., Dibble, H. L. & McPherron, S. P. in *The Cave of Fontéchevade: Recent Excavations and their Paleoanthropological Implications* (eds. Chase, P. G. et al.) 28–62 (Cambridge Univ. Press, 2009).</edb>

<jrn>40. Soressi, M. et al. Neandertals made the first specialized bone tools in Europe. *Proc. Natl Acad. Sci. USA* **110**, 14186–14190 (2013). </jrn>

<jrn>41. Richter, D. et al. The age of the hominin fossils from Jebel Irhoud, Morocco, and the origins of the Middle Stone Age. *Nature* **546**, 293–296 (2017). </jrn>

<bok>42. Sandgathe, D. M., Dibble, H. L., McPherron, S. J. P. & Goldberg, P. in *The Middle Paleolithic Site of Pech de l'Azé IV Cave and Karst Systems of the World* 1–19 (Springer, 2018).</bok>

<jrn>43. Sinet-Mathiot, V. et al. Combining ZooMS and zooarchaeology to study Late Pleistocene hominin behaviour at Fumane (Italy). *Sci. Rep.* **9**, 12350 (2019). </jrn>

<jrn>44. Wilson, J., van Doorn, N. L. & Collins, M. J. Assessing the extent of bone degradation using glutamine deamidation in collagen. *Anal. Chem.* **84**, 9041–9048 (2012). </jrn>

<jrn>45. Welker, F. et al. Variations in glutamine deamidation for a Châtelperronian bone assemblage as measured by peptide mass fingerprinting of collagen. *Sci. Technol. Archaeol. Res.* **3**, 15–27 (2017). </jrn>

<jrn>46. Fewlass, H. et al. Pretreatment and gaseous radiocarbon dating of 40–100 mg archaeological bone. *Sci. Rep.* **9**, 5342 (2019). </jrn>

<jrn>47. Longin, R. New method of collagen extraction for radiocarbon dating. *Nature* **230**, 241–242 (1971). </jrn>

<jrn>48. Brown, T. A., Nelson, D. E., Vogel, J. S. & Southon, J. R. Improved collagen extraction by modified Longin method. *Radiocarbon* **30**, 171–177 (1988). </jrn>

- <jrn>49. Bronk Ramsey, C., Higham, T., Bowles, A. & Hedges, R. Improvements to the pretreatment of bone at Oxford. *Radiocarbon* **46**, 155–163 (2004). </jrn>
- <jrn>50. Brock, F., Bronk Ramsey, C. & Higham, T. Quality assurance of ultrafiltered bone dating. *Radiocarbon* **49**, 187–192 (2007). </jrn>
- <jrn>51. Wacker, L., Němec, M. & Bourquin, J. A revolutionary graphitisation system: fully automated, compact and simple. *Nucl. Instrum. Methods Phys. Res. B* **268**, 931–934 (2010). </jrn>
- <jrn>52. Wacker, L. et al. MICADAS: routine and high-precision radiocarbon dating. *Radiocarbon* **52**, 252–262 (2010). </jrn>
- <jrn>53. Korlević, P., Talamo, S. & Meyer, M. A combined method for DNA analysis and radiocarbon dating from a single sample. *Sci. Rep.* **8**, 4127 (2018). </jrn>
- <jrn>54. Wacker, L., Christl, M. & Synal, H. A. Bats: a new tool for AMS data reduction. *Nucl. Instrum. Methods Phys. Res. B* **268**, 976–979 (2010). </jrn>
- <jrn>55. Reimer, P. J. et al. IntCal13 and Marine13 radiocarbon age calibration curves 0–50,000 years cal BP. *Radiocarbon* **55**, 1869–1887 (2013). </jrn>
- <jrn>56. Bronk Ramsey, C. Bayesian analysis of radiocarbon dates. *Radiocarbon* **51**, 337–360 (2009). </jrn>
- <jrn>57. Skinner, M. M., Gunz, P., Wood, B. A. & Hublin, J.-J. Enamel–dentine junction (EDJ) morphology distinguishes the lower molars of *Australopithecus africanus* and *i. J.* *Hum. Evol.* **55**, 979–988 (2008). </jrn>
- <jrn>58. Skinner, M. M., Gunz, P., Wood, B. A., Boesch, C. & Hublin, J.-J. Discrimination of extant *Pan* species and subspecies using the enamel–dentine junction morphology of lower molars. *Am. J. Phys. Anthropol.* **140**, 234–243 (2009). </jrn>
- <jrn>59. Slon, V. et al. Neandertal and Denisovan DNA from Pleistocene sediments. *Science* **356**, 605–608 (2017). </jrn>
- <jrn>60. Glocke, I. & Meyer, M. Extending the spectrum of DNA sequences retrieved from ancient bones and teeth. *Genome Res.* **27**, 1230–1237 (2017). </jrn>
- <jrn>61. Dabney, J. & Meyer, M. Length and GC-biases during sequencing library amplification: a comparison of various polymerase-buffer systems with ancient and modern DNA sequencing libraries. *Biotechniques* **52**, 87–94 (2012). </jrn>

- <jrn>62. Kircher, M., Sawyer, S. & Meyer, M. Double indexing overcomes inaccuracies in multiplex sequencing on the Illumina platform. *Nucleic Acids Res.* **40**, e3 (2012). </jrn>
- <jrn>63. Renaud, G., Stenzel, U. & Kelso, J. Isee: adaptor trimming and merging for Illumina sequencing reads. *Nucleic Acids Res.* **42**, e141 (2014). </jrn>
- <jrn>64. Li, H. & Durbin, R. Fast and accurate long-read alignment with Burrows–Wheeler transform. *Bioinformatics* **26**, 589–595 (2010). </jrn>
- <jrn>65. Meyer, M. et al. A high-coverage genome sequence from an archaic Denisovan individual. *Science* **338**, 222–226 (2012). </jrn>
- <jrn>66. Li, H. et al. The Sequence Alignment/Map format and SAMtools. *Bioinformatics* **25**, 2078–2079 (2009). </jrn>
- <jrn>67. Meyer, M. et al. A mitochondrial genome sequence of a hominin from Sima de los Huesos. *Nature* **505**, 403–406 (2014). </jrn>
- <jrn>68. Meyer, M. et al. Nuclear DNA sequences from the Middle Pleistocene Sima de los Huesos hominins. *Nature* **531**, 504–507 (2016). </jrn>
- <jrn>69. Green, R. E. et al. A complete Neandertal mitochondrial genome sequence determined by high-throughput sequencing. *Cell* **134**, 416–426 (2008). </jrn>
- <jrn>70. Benazzi, S. et al. The makers of the Protoaurignacian and implications for Neandertal extinction. *Science* **348**, 793–796 (2015). </jrn>
- <jrn>71. Ermini, L. et al. Complete mitochondrial genome sequence of the Tyrolean Iceman. *Curr. Biol.* **18**, 1687–1693 (2008). </jrn>
- <jrn>72. Gilbert, M. T. P. et al. Paleo-Eskimo mtDNA genome reveals matrilineal discontinuity in Greenland. *Science* **320**, 1787–1789 (2008). </jrn>
- <jrn>73. Krause, J. et al. A complete mtDNA genome of an early modern human from Kostenki, Russia. *Curr. Biol.* **20**, 231–236 (2010). </jrn>
- <jrn>74. Green, R. E. et al. A draft sequence of the Neandertal genome. *Science* **328**, 710–722 (2010). </jrn>
- <jrn>75. Posth, C. et al. Deeply divergent archaic mitochondrial genome provides lower time boundary for African gene flow into Neanderthals. *Nat. Commun.* **8**, 16046 (2017). </jrn>

- <jrn>76. Prüfer, K. et al. The complete genome sequence of a Neanderthal from the Altai Mountains. *Nature* **505**, 43–49 (2014). </jrn>
- <jrn>77. Rougier, H. et al. Neandertal cannibalism and Neandertal bones used as tools in Northern Europe. *Sci. Rep.* **6**, 29005 (2016). </jrn>
- <jrn>78. Skoglund, P. et al. Separating endogenous ancient DNA from modern day contamination in a Siberian Neandertal. *Proc. Natl Acad. Sci. USA* **111**, 2229–2234 (2014). </jrn>
- <jrn>79. Krause, J. et al. The complete mitochondrial DNA genome of an unknown hominin from southern Siberia. *Nature* **464**, 894–897 (2010). </jrn>
- <jrn>80. Reich, D. et al. Genetic history of an archaic hominin group from Denisova Cave in Siberia. *Nature* **468**, 1053–1060 (2010). </jrn>
- <jrn>81. Sawyer, S. et al. Nuclear and mitochondrial DNA sequences from two Denisovan individuals. *Proc. Natl Acad. Sci. USA* **112**, 15696–15700 (2015). </jrn>
- <jrn>82. Slon, V. et al. A fourth Denisovan individual. *Sci. Adv.* **3**, e1700186 (2017). </jrn>
- <jrn>83. Horai, S. et al. Man's place in Hominoidea revealed by mitochondrial DNA genealogy. *J. Mol. Evol.* **35**, 32–43 (1992). </jrn>
- <jrn>84. Katoh, K. & Standley, D. M. MAFFT multiple sequence alignment software version 7: improvements in performance and usability. *Mol. Biol. Evol.* **30**, 772–780 (2013). </jrn>
- <jrn>85. Kumar, S., Stecher, G. & Tamura, K. MEGA7: molecular evolutionary genetics analysis version 7.0 for bigger datasets. *Mol. Biol. Evol.* **33**, 1870–1874 (2016). </jrn>
- <jrn>86. Schliep, K. P. phangorn: phylogenetic analysis in R. *Bioinformatics* **27**, 592–593 (2011). </jrn>
- <jrn>87. Kloss-Brandstätter, A. et al. HaploGrep: a fast and reliable algorithm for automatic classification of mitochondrial DNA haplogroups. *Hum. Mutat.* **32**, 25–32 (2011). </jrn>
- <jrn>88. Renaud, G., Slon, V., Duggan, A. T. & Kelso, J. Schmutzi: estimation of contamination and endogenous mitochondrial consensus calling for ancient DNA. *Genome Biol.* **16**, 224 (2015). </jrn>
- <jrn>89. Bouckaert, R. et al. BEAST 2: a software platform for Bayesian evolutionary analysis. *PLOS Comput. Biol.* **10**, e1003537 (2014). </jrn>

- <jrn>90. Darriba, D., Taboada, G. L., Doallo, R. & Posada, D. jModelTest 2: more models, new heuristics and parallel computing. *Nat. Methods* **9**, 772 (2012). </jrn>
- <jrn>91. Baele, G. et al. Improving the accuracy of demographic and molecular clock model comparison while accommodating phylogenetic uncertainty. *Mol. Biol. Evol.* **29**, 2157–2167 (2012). </jrn>
- <bok>92. Stoops, G. *Guidelines for Analysis and Description of Soil and Regolith Thin Sections, 184* (Soil Science Society of America, 2003).</bok>
- <bok>93. Courty, M. A., Goldberg, P. & Macphail, R. *Soils and Micromorphology in Archaeology, 344* (Cambridge Univ. Press, 1989).</bok>

Acknowledgements We thank the tourism association of Bacho Kiro Cave in the town of Dryanovo, the History museum – Dryanovo, the Regional History museum in the city of Gabrovo, Dryanovo town hall and V. Lafchiiski for their assistance with the fieldwork and in the laboratory; N. Spassov from the National Museum of Natural History in Sofia for cooperating and hosting researchers of our project; H. Temming and J. Honeyford for their technical assistance and S. Nagel, B. Nickel, B. Schellbach and A. Weihmann for their help with the ancient DNA laboratory procedures and sequencing. Field operations were funded by the Max Planck Society. AixMICADAS and its operation are funded by Collège de France and the EQUIPEX ASTER-CEREGE (principal investigator, E.B.). S.T. is funded by the European Research Council under the European Union’s Horizon 2020 Research and Innovation Programme (grant agreement no. 803147-951 RESOLUTION). The ancient DNA part of this study was funded by the Max Planck Society and the European Research Council (grant agreement no. 694707 to S.P.).

Author contributions J.-J.H. designed the study. T.T., N.S., V.A., S.S., R.S., Z.R. and S.P.M. collected field data; H.F., B.K., L.W. and S.T. established the radiocarbon dates; V.A. studied the micromorphology of the sediments; S.B., M.M.S. and J.-J.H. analysed hominin dental morphology; V.S.-M., L.P., F.W. and A.W. performed ZooMS; M.H., M.M. and S.P. performed mtDNA analysis; T.T., N.S., N.Z., S.S., I.K., V.D., J.M. and S.P.M. conducted the study of the lithics; G.M.S., R.S., V.P. and N.L.M. analysed the faunal assemblages and the osseous objects. J.-J.H. wrote the paper with contributions of all authors.

Competing interests The authors declare no competing interests.

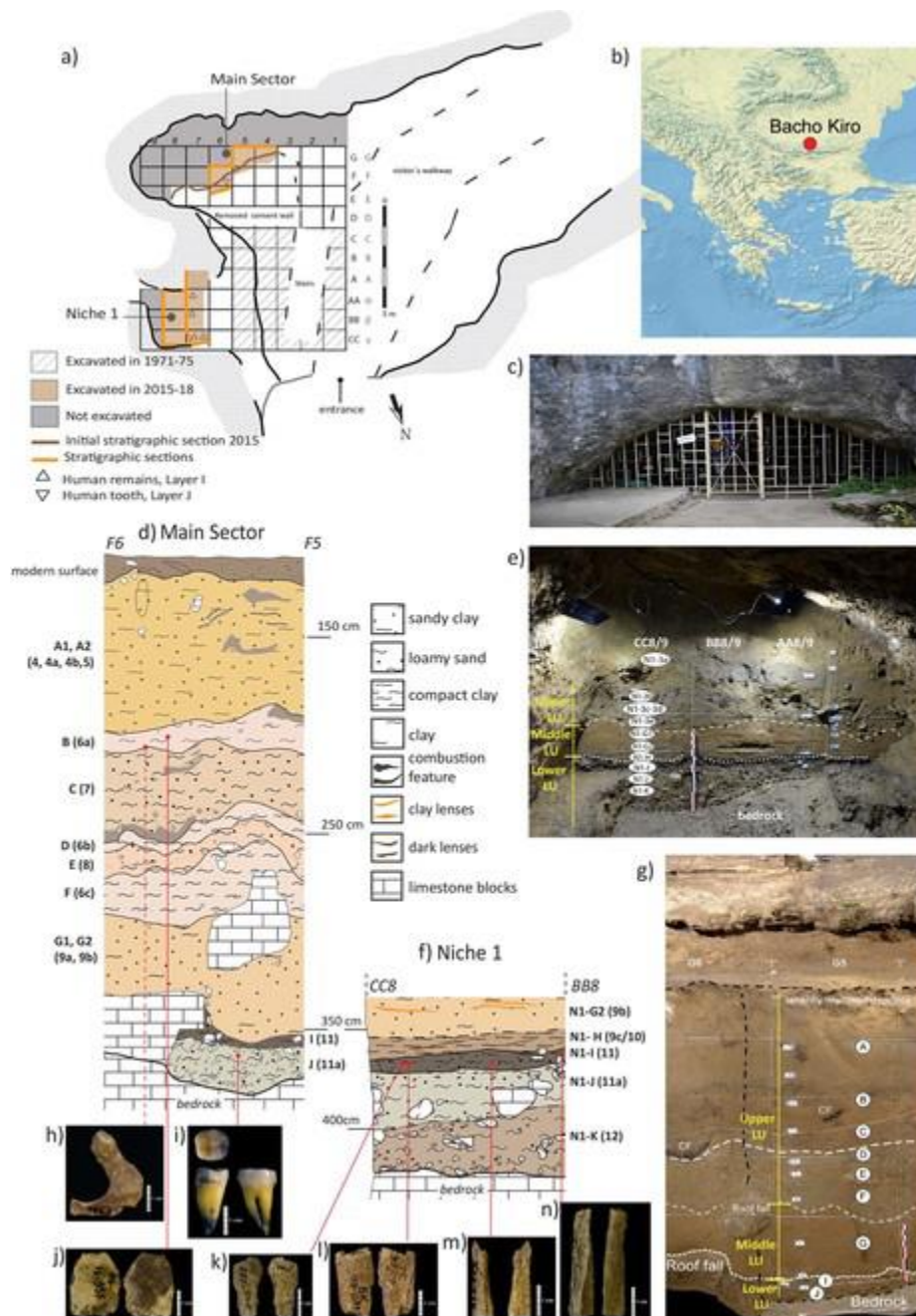
Additional information

Supplementary information is available for this paper at

Correspondence and requests for materials should be addressed to J.-J.H.

Extended Data Fig. 1 | Excavations at Bacho Kiro Cave, 2015–2018. **a**, Plan view of the entrance and the excavated areas of the cave, with the grid system of our recent excavations (letters in the left column) and those of the 1971–1975 excavations (letters in the right column). **b**, Site location in southeastern Europe. **c**, Photograph of the entrance of the cave. The floor is artificially raised; the original entrance was several metres lower than shown in this photograph. **d**, Initial stratigraphic section drawing of the exposed profile from the Main sector in 2015 (codes

for the archaeological layers are on the left, with the corresponding layers from the 1971–1975 excavations in parentheses). **e**, Frontal view of the Niche 1 sector and its stratigraphic subdivisions. **f**, Lower part of the stratigraphic section drawing of the Niche 1 sector, in 2018. Note the thickness and preservation of the lower deposits here in comparison with the Main sector profile. **g**, Photograph of the Main sector transversal section on the line F5–F6 and G5–G6 before excavation in 2015. CF, combustion feature. **h–n**, Hominin remains identified by ZooMS with their IDs: BK-1653 (**h**) and F6-597 (**j**) from layer B, with **h** coming from the 1971–1975 excavations (dashed line); BB7-240 (**k**), CC7-2289 (**l**), CC7-335 (**m**) and AA7-738 (**n**) from layer N1-I. Continuous lines connect the fossils with their find locations. **i**, Second lower molar (F6-620) from layer J in the Main sector.

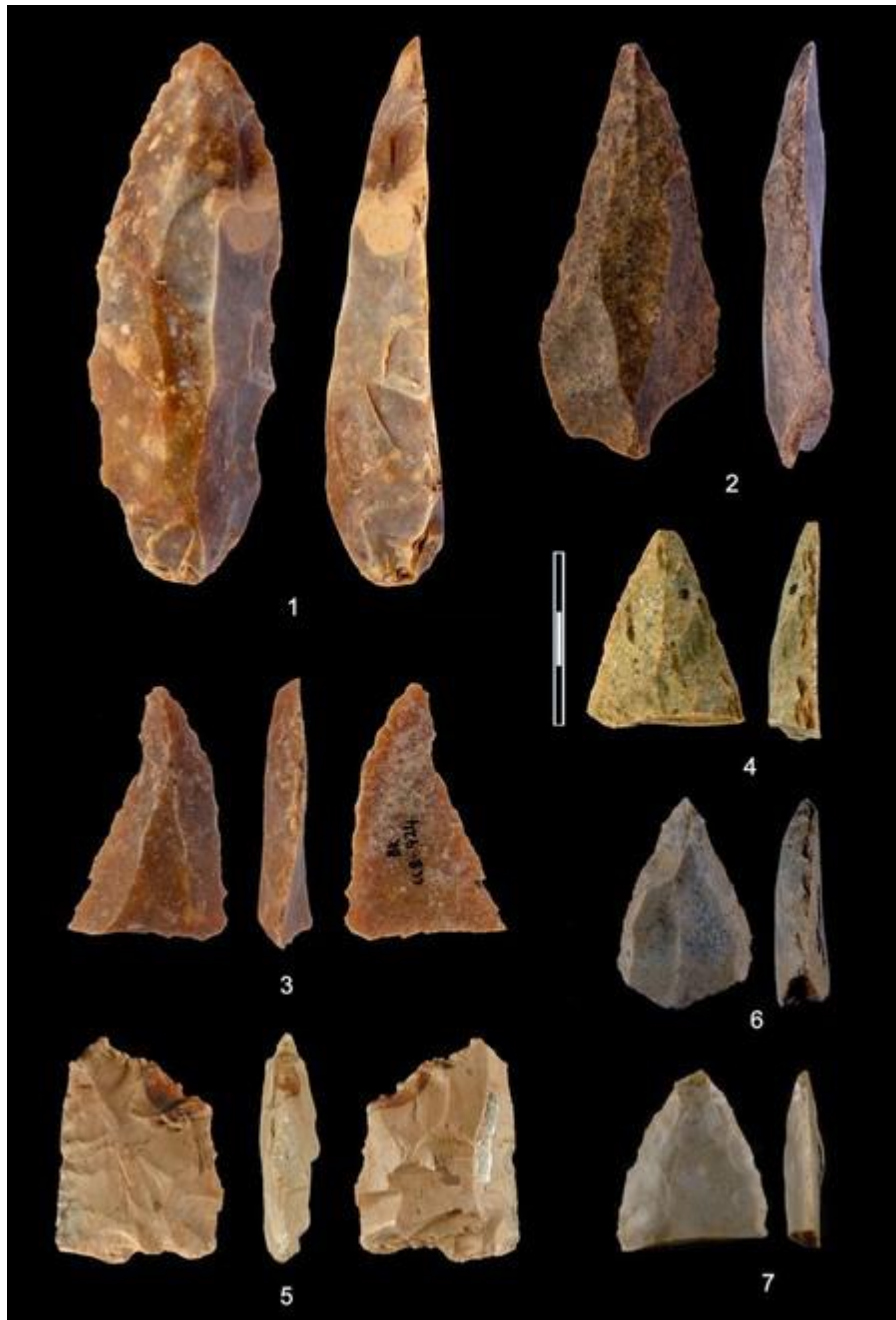


Extended Data Fig. 2 | Geographical distributions. Geographical distribution of the main IUP sites of western and central Eurasia (black dots), directly dated early *H. sapiens* predating 37,000 cal. yr BP (empty black dots) and directly dated late Neanderthals associated with Châtelperronian assemblages (orange squares). Bacho Kiro Cave is represented by a red star.



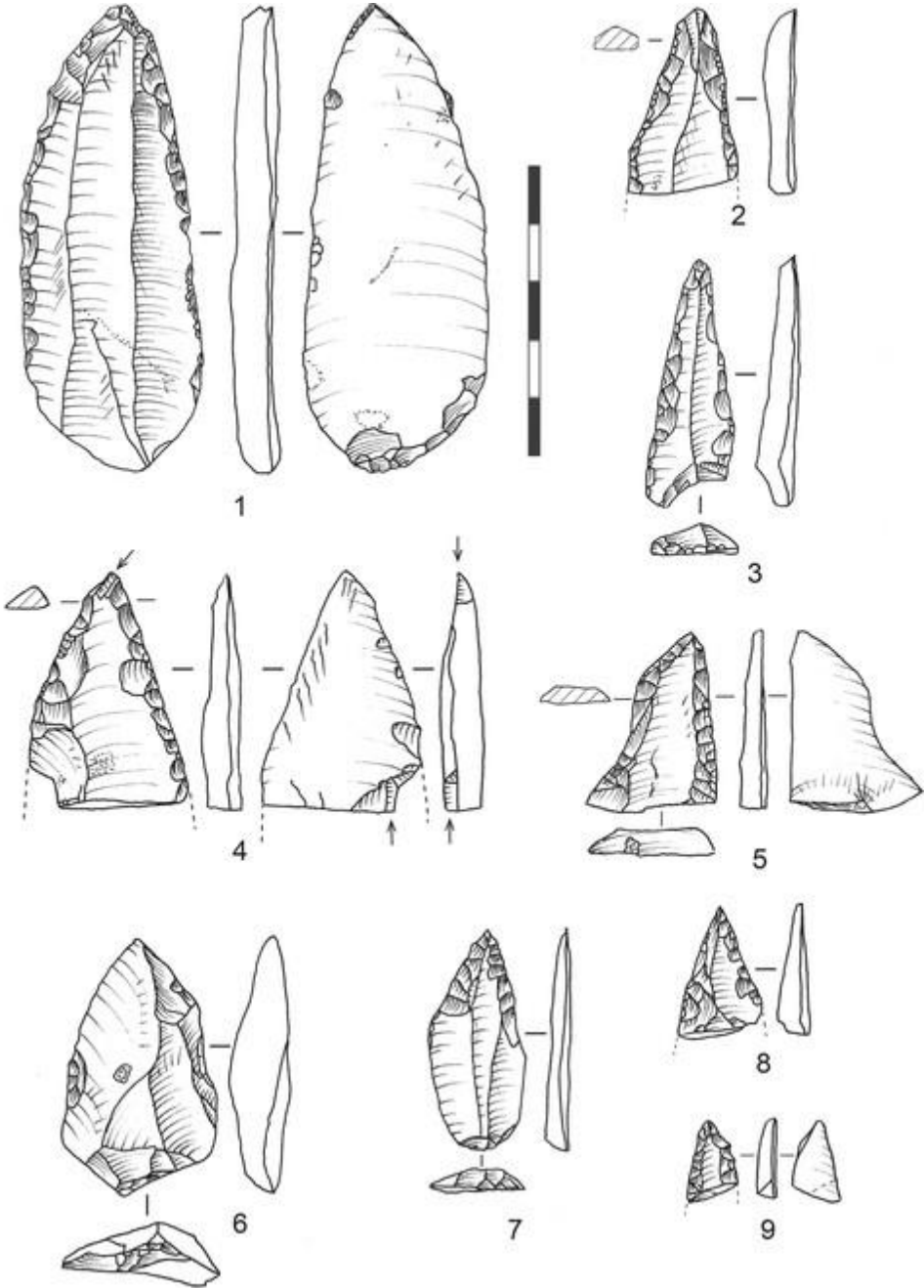
Extended Data Fig. 3 | Photographs of lithic artefacts from layer I of Bacho Kiro Cave. Pointed retouched blades and fragments (1–4, 6, 7) and piece with bifacial retouch (5).

Photographs by V.S.-M. and T. Tsanova.



Extended Data Fig. 4 | Drawings of lithic artefacts from layer I of Bacho Kiro Cave. Pointed retouched blade with slightly oblique truncation and base modified by inverse retouch (1), pointed blade fragments (2 and 5, which is has an oblique truncation and slight notch on the left edge, and was perhaps intentionally fragmented), pointed, small blades fragments (3, 7, 8), pointed blade fragment with opposing pseudo-burin blows on the apex and on the distal fracture

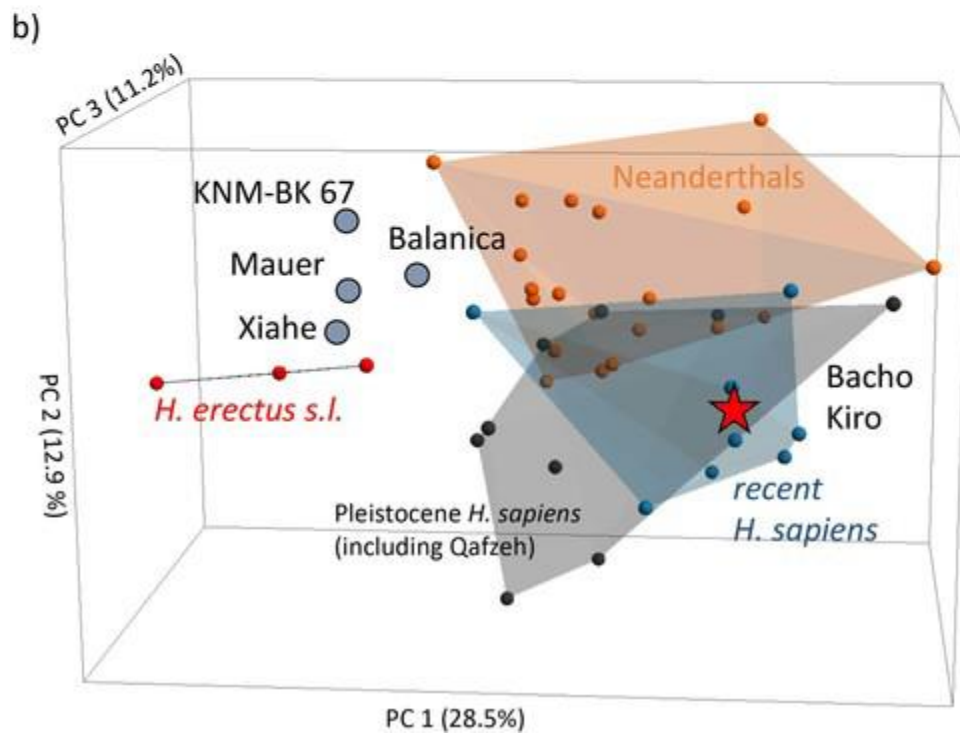
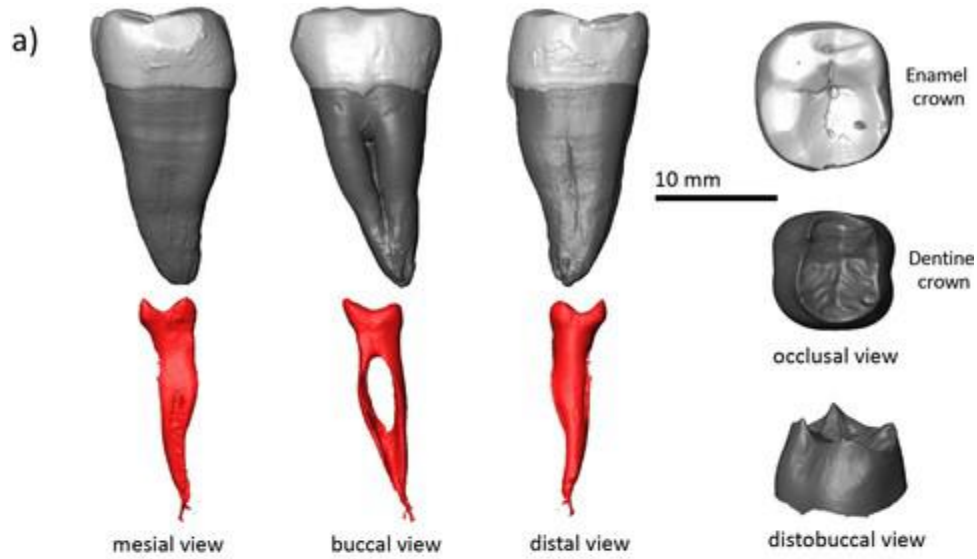
edge (perhaps indicating use as a projectile) (4) and Levallois flake (6). Drawings by I.K. and T.



Tsanova).

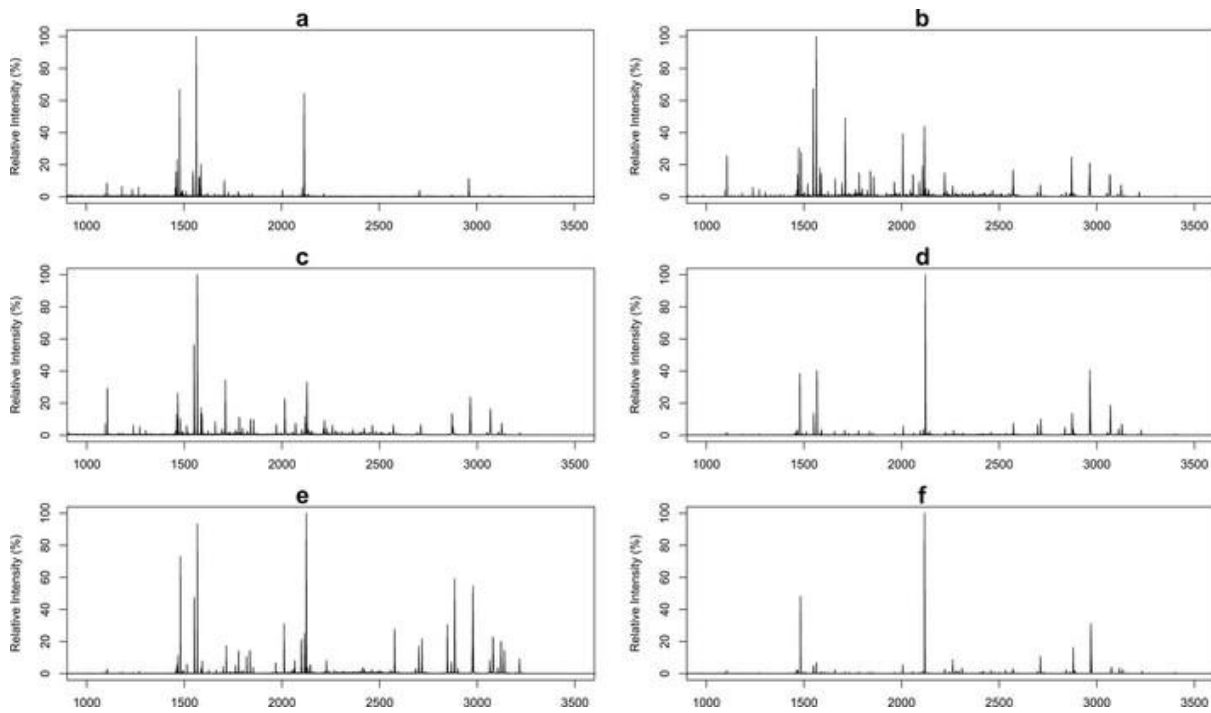
Extended Data Fig. 5 | Human lower second molar (F6-620). **a**, Mesial, buccal and distal views of the crown, root and pulp chamber (left) and occlusal views of the enamel and dentine crown (right). **b**, A principal component analysis of the shape of the enamel–dentine junction ridge and cervix places the Bacho Kiro Cave second lower molar (F6-620) within the samples of recent ($n = 8$) and Pleistocene ($n = 9$) *H. sapiens*, and outside the distribution of Neanderthals

($n = 20$) and *H. erectus* ($n = 3$).

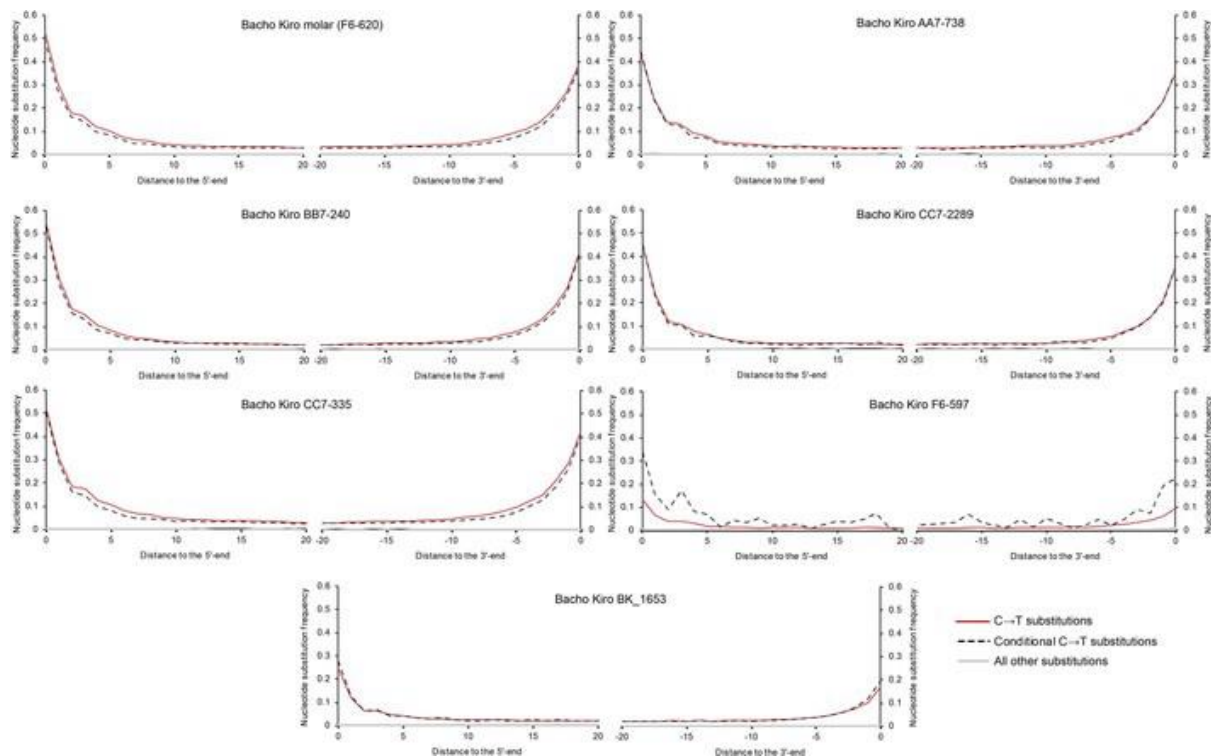


Extended Data Fig. 6 | MALDI-TOF-MS spectra for the six bone specimens identified as hominins through ZooMS analysis. a, B4-1653 (layer 6a/7). b, AA7-738 (layer N1-I). c, BB7-

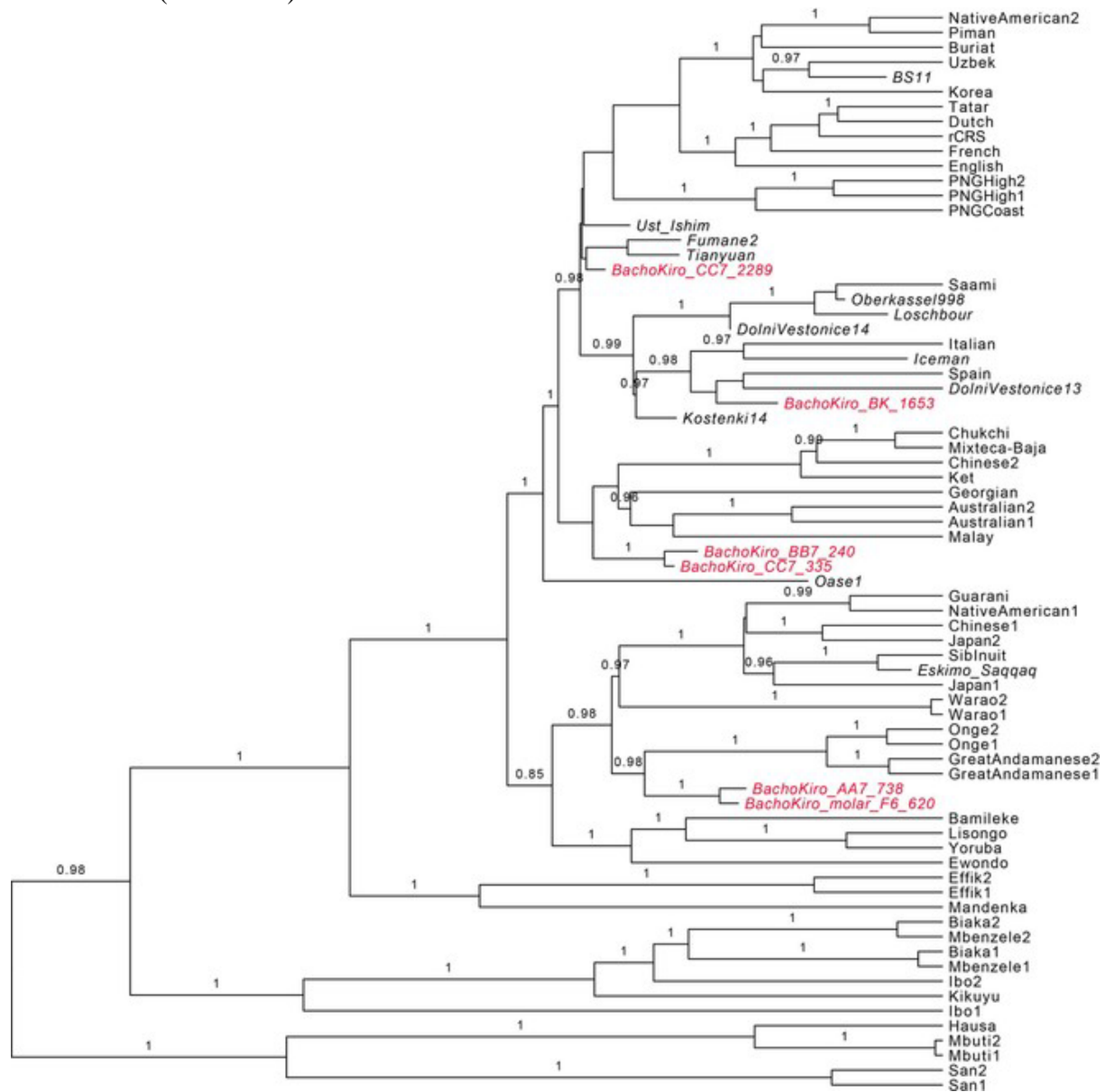
240 (layer N1-I). **d**, CC7-2289 (layer N1-I). **e**, CC7-335 (layer N1-I). **f**, F6-597 (layer B).



Extended Data Fig. 7 | Frequency of nucleotide substitutions at the beginning and the ends of mtDNA alignments for the Bacho Kiro Cave specimens. Only fragments of at least 35 base pairs in length that mapped to the revised Cambridge Reference Sequence with a mapping quality of at least 25 were used for this analysis. Solid lines in red depict all fragments and dashed lines depict the fragments that have a C-to-T substitution at the opposing end ('conditional' C-to-T substitutions). All other types of substitution are marked in grey.



Extended Data Fig. 8 | Bayesian phylogenetic tree relating Bacho Kiro Cave mtDNA to 54 present-day humans, 10 directly radiocarbon dated ancient *H. sapiens* and the Vindija 33.16 Neanderthal. The Bacho Kiro Cave specimens are in red. Other ancient *H. sapiens* used as calibration points to estimate the tip dates of Bacho Kiro Cave specimens are italicized. The posterior probabilities are denoted above the branches. The mtDNA of Vindija 33.16 was used to root the tree (not shown).



Extended Data Table 1 | Comparative dental metrics:

BL, bucco-lingual width; MD, mesiodistal length; CI, crown index (BL/MD); CCA, calculated crown area (BL × MD). Values are in mm. \bar{x} is the mean; minimum and maximum values are between the brackets; σ is the standard deviation; *n* indicates sample size. The Upper Palaeolithic *H. sapiens* sample includes individuals from the sites of: Les Abeilles, Bacho Kiro Cave, Brno, Bruniquel, Castenet, La Chaud, Dolní Věstonice, Farincourt, La Ferrassie, La Grèze, Les Rois, Isturitz, Kostenki, Kumchon, Laugerie-Basse, Lespugue, La Linde, Abri de la Madeleine, Nazlet Khater, Peștera cu Oase, Peche de la Boissiere, San Teodoro, St Germaine-la-Rivière, Sunghir, Les Vachons and Vindija. The early *H. sapiens* sample includes individuals from the sites of Border Cave, El Harhoura, Cave of Hearths, Dar es Soltane, Die Kelders, Haua Fteah, Jebel Irhoud, Klaises River Mouth, Mumba, Qafzeh, Skhul, Témará and Zhiren. The Neanderthal sample includes individuals from the sites of: Arcy-sur-Cure, Krapina, La Fate, Grotta

Guattari, Hortus, Monte Fernera, Montmaurin, Ochoz, Petit-Puymoyen, La Quina, Le Regourdou, Spy, St Césaire, Subalyuk and Tabun. The recent human sample includes archaeological specimens representing western Europe, eastern Europe, southern Europe, Japan, China, the Near East, India, the Andaman Islands, Australia, New Guinea, northern Africa, southern Africa, eastern Africa and western Africa.

Extended Data Table 2 | mtDNA branch-shortening estimates

Estimates for Bacho Kiro Cave specimens as determined in a Bayesian framework implemented in BEAST2, and by using 10 radiocarbon-dated ancient *H. sapiens* as calibration points (Supplementary Table 9).